Experimental Demonstration of a Multifunctional All-Optical Quantum State Transfer Machine

Yanbo Lou,[1,†] Shengshuai Liu,[1,†] and Jietai Jing[1,2,3,4,*]

[1]State Key Laboratory of Precision Spectroscopy, Joint Institute of Advanced Science and Technology, School of Physics and Electronic Science, East China Normal University, Shanghai 200062, China
[2]CAS Center for Excellence in Ultra-intense Laser Science, Shanghai 201800, China
[3]Department of Physics, Zhejiang University, Hangzhou 310027, China
[4]Collaborative Innovation Center of Extreme Optics, Shanxi University, Taiyuan, Shanxi 030006, China

(Received 24 October 2020; revised 29 March 2021; accepted 17 May 2021; published 28 May 2021)

Quantum information protocol with quantum resources shows a great advantage in substantially improving security, fidelity, and capacity of information processing. Various quantum information protocols with diverse functionalities have been proposed and implemented. However, in general, the present quantum information system can only carry out a single information protocol or deal with a single communication task, which limits its practical application in the future. Therefore, it is essential to develop a multifunctional platform compatible with multiple different quantum information protocols. In this Letter, by utilizing an all-optical platform consisting of a gain-tunable parametric amplifier, a beam splitter, and an entanglement source, we experimentally realize the partially disembodied quantum state transfer protocol, which links the all-optical quantum teleportation protocol and the optimal $1 \rightarrow N$ coherent state cloning protocol. As a result, these three protocols, which have different physical essences and functionalities, are implemented in a single all-optical machine. In particular, we demonstrate that the partially disembodied quantum state transfer protocol can enhance the state transfer fidelity compared with all-optical quantum teleportation under the same strength of entanglement. Our all-optical quantum state transfer machine paves a way to implement the multifunctional quantum information system.

DOI: 10.1103/PhysRevLett.126.210507

Quantum information protocol aims to exploit the fundamental principles of quantum physics to develop high security, high fidelity, and high capacity information generation, transmission, and processing methods beyond the classical information system [1–3], which has attracted great attentions all over the world. With the extensive and in-depth study on it, numerous quantum information protocols with different functionalities have been developed, such as quantum teleportation [4–14], quantum dense coding [15,16], quantum secret sharing [17], and quantum cloning [18–21], which cannot be implemented in the classical information system.

In general, the current quantum information system can only carry out a single information protocol or deal with a single communication task. However, the quantum information task cannot be immutable. Therefore, it is essential to develop a multifunctional platform compatible with multiple different quantum information protocols for the practical application of quantum information in the future. In this Letter, we propose an all-optical quantum state transfer machine (QSTM), which consists of a gain-tunable parametric amplifier based on four-wave mixing (FWM) process in a ^{85}Rb atomic ensemble [22–30], a beam splitter and an Einstein-Podolsky-Rosen (EPR) entangled source [31]. We show that this device can implement the all-optical partially disembodied quantum state transfer (PDQST) protocol [32]. We experimentally demonstrate that the PDQST protocol can enhance state transfer fidelity under the same strength of entanglement compared with all-optical quantum teleportation (AOQT). More importantly, the all-optical PDQST protocol links two other different all-optical protocols, i.e., AOQT [12,13] and all-optical optimal $1 \rightarrow N$ coherent state cloning (CSC). The implementation of three different protocols in a single all-optical platform shows the multifunctionality of our all-optical machine.

The schematic of our all-optical machine for implementing deterministic quantum state transfer is shown in Fig. 1. EPR entangled state is generated by a nondegenerate FWM process (FWM_1) pumped with a pump beam ($pump_1$). The two modes of the EPR entangled state are sent to Alice and Bob through two optical channels, respectively. Then, Alice implements a gain-tunable parametric amplification on the unknown input state $\hat{a}_{\text{in}}$ with one half of the EPR entangled state $\hat{b}_1$ by a second FWM process (FWM_2) pumped with another pump beam ($pump_2$). For such a parametric amplifier based on FWM_2 with tunable amplification gain of G, one of the outputs is given by

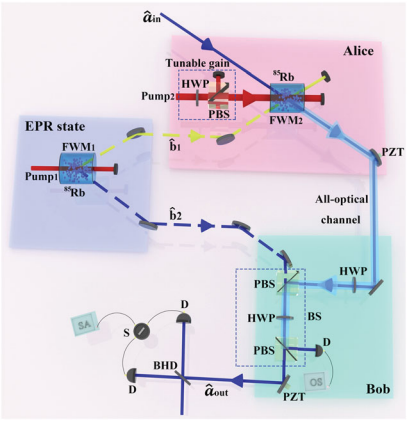

FIG. 1. The experimental layout for multifunctional all-optical QSTM. EPR state ($\hat{b}_1$ and $\hat{b}_2$), Einstein-Podolsky-Rosen entangled state; HWP, half-wave plate; PBS, polarization beam splitter; D, detector; BS, beam splitter with adjustable transmissivity; BHD, balanced homodyne detection; FWM, four-wave mixing process; PZT, piezoelectric transducer; S, subtractor; SA, spectrum analyzer; OS, oscilloscope; $\hat{a}_{in}$, input state; $\hat{a}_{out}$, output state; pump_1 and pump_2, the pump beams for FWM_1 and FWM_2.

$$\hat{a}_{amp} = \sqrt{G}\hat{a}_{in} + \sqrt{G-1}\hat{b}_1^{\dagger}. \tag{1}$$

Then, Alice sends the amplified state $\hat{a}_{amp}$ to Bob through an all-optical channel. In order to characterize the loss effect in the all-optical channel, we model the channel loss by a beam splitter which introduces a vacuum state $\hat{v}_0$ [33]. Therefore, the amplified state can be expressed as

$$\begin{aligned}\hat{a}_{loss} &= \sqrt{1-\eta}\hat{a}_{amp} + \sqrt{\eta}\hat{v}_0, \\ &= \sqrt{1-\eta}\left(\sqrt{G}\hat{a}_{in} + \sqrt{G-1}\hat{b}_1^{\dagger}\right) + \sqrt{\eta}\hat{v}_0,\end{aligned} \tag{2}$$

where η denotes the loss rate of the all-optical channel. Then, Bob implements a state displacement by combining the amplified state and the other half of the EPR entangled state $\hat{b}_2$ through a beam splitter (BS) with adjustable transmissivity ε, which consists of two polarization beam splitters (PBS) and one half-wave plate (HWP). Consequently, the output field reads $\hat{a}_{out} = \sqrt{\varepsilon}\hat{a}_{loss} - \sqrt{1-\varepsilon}\hat{b}_2$. Under the condition of transmissivity $\varepsilon = [1/G(1-\eta)]$, the final output state can be expressed as

$$\begin{aligned}\hat{a}_{out} = \hat{a}_{in} &+ \sqrt{\frac{G-1}{G}}\left(\hat{b}_1^{\dagger} - \sqrt{\frac{G(1-\eta)-1}{(1-\eta)(G-1)}}\hat{b}_2\right) \\ &+ \sqrt{\frac{\eta}{G(1-\eta)}}\hat{v}_0\end{aligned} \tag{3}$$

(see Sec. C of Supplemental Material for a detailed derivation [34]). In the end, Victor accomplishes the verification of quantum state transfer.

Generally, the fidelity $F \in [0,1]$ of the reconstructed state compared with the input state can be used to characterize the performance of a quantum information protocol. The fidelity can be defined as the overlap between the input and output states and has the form of

$$F = \frac{2}{\sigma_Q}\exp\left[-\frac{2}{\sigma_Q}|\beta_{out} - \beta_{in}|^2\right], \tag{4}$$

where

$$\sigma_Q = \sqrt{(1+\sigma_W^X)(1+\sigma_W^Y)}. \tag{5}$$

σ_Q is the variance of the output state in representation of the Q function, σ_W^X and σ_W^Y are the variances of the Wigner distribution corresponding to the amplitude and phase quadratures of the output state. β_{in} and β_{out} are amplitudes of the input state at Alice and the output state at Bob, respectively. For our all-optical QSTM, the final output state is given by Eq. (3) above. In order to better illustrate the physical essence differences of the three all-optical protocols, we consider the ideal case without taking into account the channel loss. In this way, the output state can be expressed as

$$\hat{a}_{out} = \hat{a}_{in} + \sqrt{\frac{G-1}{G}}(\hat{b}_1^{\dagger} - \hat{b}_2). \tag{6}$$

Then, we can get

$$\sigma_W^X = \sigma_W^Y = 1 + \frac{2(G-1)}{G}(\sqrt{H} - \sqrt{H-1})^2, \tag{7}$$

where H is the parametric gain for the generation of EPR entanglement. Consequently, its fidelity can be given as

$$F = \frac{1}{1 + \frac{G-1}{G}(\sqrt{H} - \sqrt{H-1})^2}. \tag{8}$$

First, with the fixed entanglement strength, i.e., fixed parametric gain H, the smaller the amplification gain of the parametric amplifier G is, the higher the fidelity of the output state will be. That is to say, one can efficiently enhance the fidelity of quantum state transfer by decreasing the amplification gain G of the parametric amplifier. Under such a condition, our all-optical machine is equivalent to the PDQST protocol originally proposed in a theoretical work [32]. Second, with the amplification gain $G \gg 1$, Eq. (8) reduces to

$$F_{AOQT} \approx \frac{1}{1 + (\sqrt{H} - \sqrt{H-1})^2}. \tag{9}$$

Under such a condition, our all-optical QSTM implements the AOQT protocol [12,13]. Third, when the sender Alice

and the receiver Bob do not share EPR entanglement ($H = 1$), Eq. (8) reduces to

$$F_{\text{clone}} = \frac{G}{2G-1}. \tag{10}$$

Under such a condition, our all-optical machine realizes the optimal $1 \to N$ CSC protocol in continuous-variable (CV) regime [18–21], where N equals the amplification gain G of the parametric amplifier. Therefore, it can be clearly seen that the PDQST protocol can link AOQT protocol and optimal $1 \to N$ CSC protocol by operating the all optical QSTM at different conditions, explicitly showing its multifunctionality. It should be noted that the fidelity of the PDQST protocol can beat the optimal $1 \to N$ CSC protocol with any parametric gain $H > 1$. In other words, the fidelity of optimal $1 \to N$ CSC protocol is the classical limit of the PDQST protocol. In particular, when $N(G) \gg 1$, the fidelity of optimal $1 \to N$ CSC is 0.5, which corresponds to the classical limit of AOQT.

In experiment, Alice uses a gain-tunable parametric amplifier based on a FWM in ^{85}Rb to amplify the input state and then sends the amplified state to Bob through an all-optical channel. Bob adjusts the transmissivity of the BS according to the amplification gain, which ensures that the first-order moments of the input and output states are the same ($|\beta_{\text{out}} - \beta_{\text{in}}| = 0$). Finally, Victor accomplishes the verification of quantum state transfer by balanced homodyne detection (BHD) (see Sec. A of Supplemental Material for a detailed explanation [34]). The typical results of our QSTM for realizing these three all-optical protocols are shown in Fig. 2. First of all, we show the results for realizing the PDQST protocol by setting the amplification gain $G = 2$. Figure 2(a) [Figure 2(b)] indicates the situation where Victor locks the phase of BHD at 0 ($\pi/2$), corresponding to the measurement of the amplitude quadrature $\hat{X} = \hat{a}^\dagger + \hat{a}$ [phase quadrature $\hat{Y} = i(\hat{a}^\dagger - \hat{a})$] of the input and output states. Here, $\hat{a}$ and $\hat{a}^\dagger$ are annihilation and creation operators of the corresponding optical field. The noise levels of the input state are measured by blocking all the pump beams, which are shown as green traces in Figs. 2(a) and 2(b). Then, if pump$_1$ is blocked while pump$_2$ is open, i.e., the EPR entanglement is blocked while parametric amplifier is in operation, the optimal $1 \to 2$ CSC is implemented. In this case, the measured noise powers of the output state [blue traces in Figs. 2(a) and 2(b)] are 3.17 ± 0.10 dB above the corresponding noise level of the input state, giving a fidelity F of 0.65 ± 0.01. Then, with both pump$_1$ and pump$_2$ open and scanning the relative phase between $\hat{b}_1$ and $\hat{b}_2$ by a piezoelectric transducer (PZT), the minima of the red traces in Figs. 2(a) and 2(b) of the output state noise power measured by Victor are 2.21 ± 0.18 dB and 2.17 ± 0.19 dB above the corresponding green traces. This gives a fidelity F of 0.75 ± 0.02, beating the measured fidelity of the corresponding optimal $1 \to 2$ CSC and showing the successful implementation of the PDQST protocol.

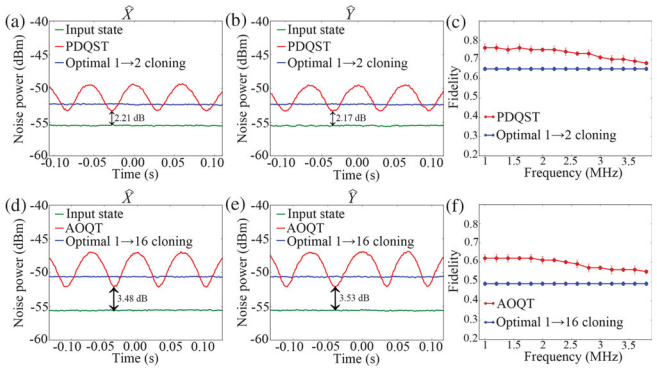

FIG. 2. Noise powers of the output state measured by Victor's BHD. (a) [(b)], measurement of amplitude (phase) quadrature with an amplification gain of 2. (d) [(e)], the measurement of amplitude (phase) quadrature with an amplification gain of 16. (c) [(f)], fidelities versus the sideband frequency with an amplification gain of 2 (16). The analysis frequency is set to 1.4 MHz for (a), (b), (d), and (e). The error bars are obtained from the standard deviations of multiple repeated measurements.

As a comparison, we measure the noise power under the same strength of entanglement at the parametric gain $G = 16 \gg 1$, which corresponds to the implementation of AOQT. Figure 2(d) [Fig. 2(e)] indicates the situation where Victor locks the phase of BHD at 0 ($\pi/2$), corresponding to the measurement of amplitude (phase) quadrature. The green traces indicate the noise level of the input state. The blue traces indicate the noise level of the output state of the optimal $1 \to 16$ CSC, which are 4.89 ± 0.11 dB above the corresponding green traces, giving a fidelity F of 0.49 ± 0.01. Since the amplification gain $16 \gg 1$, its fidelity can be approximated as the classical limit of AOQT. In fact, the theoretically predicted fidelity of the optimal $1 \to 16$ CSC is 0.516, which is already very close to the classical limit (0.5) of AOQT. Therefore, it is reasonable to treat the optimal $1 \to 16$ cloning limit as the classical limit for evaluating the success of AOQT in experiment. The minima of the red traces in Figs. 2(d) and 2(e) indicate the noise level of the output state of AOQT, which are 3.48 ± 0.20 dB and 3.53 ± 0.19 dB above the corresponding green traces. This gives a fidelity F of 0.62 ± 0.02, beating the fidelity of the experimentally measured classical limit and showing the successful implementation of AOQT protocol. From Fig. 2, it is obvious that the output state noise power [the minima of the red traces in Fig. 2(a) and Fig. 2(b)] of the PDQST protocol is notably lower than that of AOQT [the minima of the red traces in Fig. 2(d) and Fig. 2(e)], clearly showing the ability of the PDQST protocol for enhancing state transfer fidelity compared with AOQT. In fact, the fidelity of the output state is enhanced from 0.62 to 0.75 under the same strength of entanglement.

Since our platform is all optical, which avoids the optic-electro and electro-optic conversions in standard CV

quantum information protocols [14], it is worth showing the bandwidth of information that an all-optical platform can transfer. For this purpose, we also experimentally demonstrate its broadband property. We increase the analysis frequency from 1 to 3.8 MHz with intervals of 0.2 MHz under the same experimental conditions. The experimental results are shown in Figs. 2(c) and 2(f). The red traces in Figs. 2(c) and 2(f) show the state transfer fidelities of the PDQST protocol and AOQT protocol versus analysis frequency, respectively. The blue traces in Figs. 2(c) and 2(f) show the fidelities of the optimal $1 \rightarrow 2$ and $1 \rightarrow 16$ CSC protocols, respectively. It can be seen that the fidelities of the PDQST protocol and AOQT protocol decrease with the increasing of the sideband frequency while the fidelities of the optimal $1 \rightarrow 2$ and $1 \rightarrow 16$ CSC protocols keep constant. This is due to the fact that the strength of EPR entanglement from FWM process shared by Alice and Bob decreases with the increasing of the sideband frequency (see Sec. B of Supplemental Material for a detailed explanation [34]) and there is no EPR entanglement involved for the optimal $1 \rightarrow N$ CSC. Nevertheless, the results in Figs. 2(c) and 2(f) clearly show that quantum state transfer can be successfully accomplished in our all-optical QSTM as long as the state transfer sideband is within the bandwidth of the entanglement. Recently, the THz-bandwidth CV squeezed light has been demonstrated through an all-optical phase-sensitive detection [38], with which the broadband all-optical quantum state transfer is promising for practical applications in the future.

The optical channel of the PDQST protocol is semiquantum [32], and therefore, the channel loss will affect the fidelity of the output state. To show such a loss effect, we measure state transfer fidelities of the PDQST protocol and AOQT protocol as functions of channel losses. As shown in Fig. 3, when the amplification gain is large enough ($G = 16$), corresponding to AOQT protocol, the state transfer fidelity is tolerant to channel loss (trace A). It means that the all-optical channel of AOQT is closer to a classical channel. This is very critical for realizing long-distance quantum state transfer because large channel loss is inevitable in practical long-distance optical channels. Such a loss-tolerant advantage can also ensure the integration and compatibility of the AOQT protocol with the modern optical communication systems. In contrast, when the amplification gain is not large enough ($G = 2$), corresponding to the PDQST protocol, the state transfer fidelity quickly drops as the channel loss increases (trace B), indicating that the all-optical channel is not a classical channel anymore. Although the PDQST protocol sacrifices the loss-tolerant advantage, it can achieve higher state transfer fidelity in the low loss region with the same strength of entanglement compared with AOQT protocol as indicated by both experiment (red and blue dotted traces) and theory (red and blue solid traces). For low-loss situations, where channel loss tolerance is not strictly required, such as on-chip quantum state transfer [39], the PDQST protocol serves as a promising way to enhance state transfer fidelity. In a word, our all-optical QSTM can be operated as different protocols in different application scenarios for either enhancing state transfer fidelity or increasing state transfer distance.

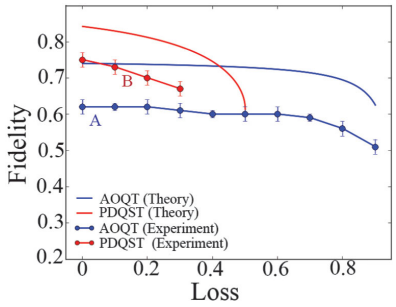

FIG. 3. Fidelities as functions of channel loss. The blue and red dotted traces represent the experimentally measured state transfer fidelities versus channel loss when amplification gain is 16 and 2, respectively. The analysis frequency is set to 1.4 MHz. The error bars are obtained from the standard deviations of multiple repeated measurements.

In order to better illustrate the multifunctionality of our all-optical QSTM, we measure the state transfer fidelities of three different all-optical protocols according to Eqs. (8)–(10). We increase amplification gain G from 1.5 to 16 and for each gain; we measure state transfer fidelities of the output state with (red dotted trace) and without (blue dotted trace) entanglement as shown in Fig. 4. Specifically, the blue dotted trace indicates the output state fidelity of the optimal $1 \rightarrow N$ CSC protocol as a function of G and the red dotted trace indicates state transfer fidelity of the PDQST protocol as a function of G, which is equivalent to AOQT for amplification gain $G \gg 1$. The corresponding theoretical curves are given by the solid traces of the same colors.

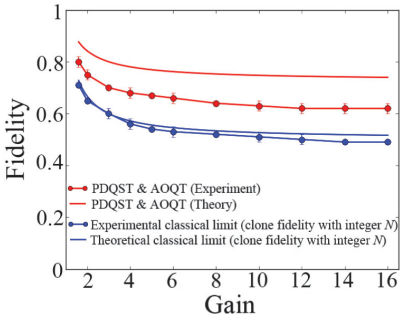

FIG. 4. Fidelities as functions of G for the multifunctional all-optical QSTM. The red and blue dotted traces represent the experimentally measured state transfer fidelities of the PDQST protocol (equivalent to AOQT for amplification gain $G \gg 1$), optimal $1 \rightarrow N$ CSC protocol, respectively, as functions of G. The analysis frequency is set to 1.4 MHz. The error bars are obtained from the standard deviations of multiple repeated measurements.

From Fig. 4, we can find that with the decreasing of G, state transfer fidelities increase. For the same amplification gain G, due to the help of EPR entanglement, the fidelity of the PDQST protocol is always better than the fidelity of optimal $1 \to N$ CSC. In particular, we achieve a fidelity of 0.80 ± 0.02 for retrieving a coherent state when the amplification gain G is set to 1.5 by the PDQST protocol. These results clearly demonstrate the ability of the PDQST protocol for enhancing state transfer fidelity. The measured fidelity of optimal $1 \to N$ CSC (blue dotted trace) is in good agreement with the theoretically predicted value (blue solid trace). The slight deviation between them at high amplification gain is caused by extra noise from the pump scattering and higher-order irrelevant nonlinear processes [33]. The measured fidelities of the PDQST and AOQT protocols (red dotted trace) have a similar trend with the theoretically predicted value (red solid trace). These results in Fig. 4 also clearly show the multifunctionality of our all-optical QSTM.

It is worth noting that the relatively large deviations between theory and our experimental results of AOQT and the PDQST protocol in Figs. 3 and 4 are mainly due to the deviation between the inseparabilities of experimentally generated entanglement and theoretically predicted entanglement (see Sec. B of Supplemental Material for a detailed explanation and the possible ways for increasing the fidelity [34]).

In conclusion, we have experimentally demonstrated the all-optical PDQST protocol. In particular, we demonstrate the ability of the PDQST protocol for enhancing state transfer fidelity compared with AOQT. Specifically, the fidelity is enhanced from 0.62 to 0.80 under the same strength of entanglement. Enhancing the fidelity by introducing a noiseless linear amplifier at the expense of deterministic advantage of CV system has been studied by several groups [40–43]. By contrast, the PDQST protocol studied here enhances the fidelity by introducing a semiquantum channel without sacrificing the deterministic advantage of CV system. In addition, we have also shown the broadband characteristic of our all-optical platform, which is essential for realizing a high-capacity quantum communication network and high-speed quantum computing in the future [14]. More importantly, it is the all-optical PDQST protocol which links AOQT and all-optical optimal $1 \to N$ CSC protocols. These three all-optical protocols integrated in a single device have different physical essences and functions, showing the multifunctionality of our all-optical QSTM. Recently, it is a new trend to realize CV quantum information system by integrated optical devices, such as a silicon nitride nanophotonic device [44–47] and periodically poled lithium niobate waveguide [38,48,49]. In the future, combining these integrated CV quantum optical devices is a promising way for implementing a fully integrated all-optical multifunctional QSTM.

This work was funded by Innovation Program of Shanghai Municipal Education Commission (Grant No. 2021-01-07-00-08-E00100); the National Natural Science Foundation of China (No. 11874155, No. 91436211, No. 11374104); Basic Research Project of Shanghai Science and Technology Commission (No. 20JC1416100); Natural Science Foundation of Shanghai (No. 17ZR1442900); Minhang Leading Talents (201971); Program of Scientific and Technological Innovation of Shanghai (No. 17JC1400401); National Basic Research Program of China (No. 2016YFA0302103); Shanghai Municipal Science and Technology Major Project (No. 2019SHZDZX01); Shanghai Sailing Program (No. 21YF1410800); the 111 project (No. B12024); ECNU Academic Innovation Promotion Program for Excellent Doctoral Students (Grant No. YBNLTS2020-046).

*Corresponding author.
jtjing@phy.ecnu.edu.cn
†These authors contributed equally to this work.

[1] S. L. Braunstein and P. van Loock, Rev. Mod. Phys. **77**, 513 (2005).
[2] J. W. Pan, Z. B. Chen, C. Y. Lu, H. Weinfurter, A. Zeilinger, and M. Zukowski, Rev. Mod. Phys. **84**, 777 (2012).
[3] H. J. Kimble, Nature (London) **453**, 1023 (2008).
[4] C. H. Bennett, G. Brassard, C. Crépeau, R. Jozsa, A. Peres, and W. K. Wootters, Phys. Rev. Lett. **70**, 1895 (1993).
[5] D. Bouwmeester, J. Pan, M. Klaus, E. Manfred, W. Harald, and Z. Anton, Nature (London) **390**, 575 (1997).
[6] S. L. Braunstein and H. J. Kimble, Phys. Rev. Lett. **80**, 869 (1998).
[7] A. Furusawa, J. L. Sorensen, S. L. Braunstein, C. A. Fuchs, H. J. Kimble, and E. S. Polzik, Science **282**, 706 (1998).
[8] J. F. Sherson, H. Krauter, R. K. Olsson, B. Julsgaard, K. Hammerer, I. Cirac, and E. S. Polzik, Nature (London) **443**, 557 (2006).
[9] M. Riebe, H. Häffner, C. F. Roos, W. Hänsel, J. Benhelm, G. P. T. Lancaster, T. W. Körber, C. Becher, F. SchmidtKaler, D. F. V. James, and R. Blatt, Nature (London) **429**, 734 (2004).
[10] S. Olmschenk, D. N. Matsukevich, P. Maunz, D. Hayes, L. M. Duan, and C. Monroe, Science **323**, 486 (2009).
[11] F. Bussiéres, C. Clausen, A. Tiranov, B. Korzh, V. B. Verma, S. W. Nam, F. Marsili, A. Ferrier, P. Goldner, H. Herrmann *et al.*, Nat. Photonics **8**, 775 (2014).
[12] S. Liu, Y. Lou, and J. Jing, Nat. Commun. **11**, 3875 (2020).
[13] T. C. Ralph, Opt. Lett. **24**, 348 (1999).
[14] S. Takeda and A. Furusawa, APL Photonics **4**, 060902 (2019).
[15] K. Mattle, H. Weinfurter, P. G. Kwiat, and A. Zeilinger, Phys. Rev. Lett. **76**, 4656 (1996).
[16] X. Y. Li, Q. Pan, J. T. Jing, J. Zhang, C. D. Xie, and K. C. Peng, Phys. Rev. Lett. **88**, 047904 (2002).

[17] M. Hillery, V. Bužek, and A. Berthiaume, Phys. Rev. A **59**, 1829 (1999).
[18] S. L. Braunstein, N. J. Cerf, S. Iblisdir, P. van Loock, and S. Massar, Phys. Rev. Lett. **86**, 4938 (2001).
[19] J. Fiurášek, Phys. Rev. Lett. **86**, 4942 (2001).
[20] N. J. Cerf, A. Ipe, and X. Rottenberg, Phys. Rev. Lett. **85**, 1754 (2000).
[21] U. L. Andersen, V. Josse, and G. Leuchs, Phys. Rev. Lett. **94**, 240503 (2005).
[22] C. F. McCormick, V. Boyer, E. Arimonda, and P. D. Lett, Opt. Lett. **32**, 178 (2007).
[23] V. Boyer, A. M. Marino, R. C. Pooser, and P. D. Lett, Science **321**, 544 (2008).
[24] A. M. Marino, R. C. Pooser, V. Boyer, and P. D. Lett, Nature (London) **457**, 859 (2009).
[25] R. C. Pooser, A. M. Marino, V. Boyer, K. M. Jones, and P. D. Lett, Phys. Rev. Lett. **103**, 010501 (2009).
[26] S. Liu, Y. Lou, and J. Jing, Phys. Rev. Lett. **123**, 113602 (2019).
[27] K. Zhang, W. Wang, S. Liu, X. Pan, J. Du, Y. Lou, S. Yu, S. Lv, N. Treps, C. Fabre, and J. Jing, Phys. Rev. Lett. **124**, 090501 (2020).
[28] X. Pan, S. Yu, Y. Zhou, K. Zhang, K. Zhang, S. Lv, S. Li, W. Wang, and J. Jing, Phys. Rev. Lett. **123**, 070506 (2019).
[29] S. Li, X. Pan, Y. Ren, H. Liu, S. Yu, and J. Jing, Phys. Rev. Lett. **124**, 083605 (2020).
[30] R. C. Pooser, N. Savino, E. Batson, J. L. Beckey, J. Garcia, and B. J. Lawrie, Phys. Rev. Lett. **124**, 230504 (2020).
[31] A. Einstein, B. Podolsky, and N. Rosen, Phys. Rev. **47**, 777 (1935).
[32] J. Zhang, C. Xie, and K. Peng, Phys. Rev. Lett. **95**, 170501 (2005).
[33] C. F. McCormick, A. M. Marino, V. Boyer, and P. D. Lett, Phys. Rev. A **78**, 043816 (2008).
[34] See Supplemental Material at http://link.aps.org/supplemental/10.1103/PhysRevLett.126.210507 for detailed experimental setup for all-optical quantum state transfer machine, the inseparability and quantum state transfer fidelity, and loss tolerance of all-optical channel, which includes Refs. [35–37].
[35] L. M. Duan, G. Giedke, J. I. Cirac, and P. Zoller, Phys. Rev. Lett. **84**, 2722 (2000).
[36] R. Simon, Phys. Rev. Lett. **84**, 2726 (2000).
[37] J. Xin, J. Qi, and J. Jing, Opt. Lett. **42**, 366 (2017).
[38] N. Takanashi, A. Inoue, T. Kashiwazaki, T. Kazama, K. Enbutsu, R. Kasahara, T. Umeki, and A. Furusawa, Opt. Express **28**, 34916 (2020).
[39] D. Llewellyn *et al.*, Nat. Phys. **16**, 148 (2020).
[40] T. C. Ralph and A. P. Lund, AIP Conf. Proc. **1110**, 155 (2009).
[41] G. Y. Xiang, T. C. Ralph, A. P. Lund, N. Walk, and G. J. Pryde, Nat. Photonics **4**, 316 (2010).
[42] J. Y. Haw, J. Zhao, J. Dias, S. M. Assad, M. Bradshaw, R. Blandino, T. Symul, T. C. Ralph, and P. K. Lam, Nat. Commun. **7**, 13222 (2016).
[43] A. E. Ulanov, I. A. Fedorov, A. A. Pushkina, Y. V. Kurochkin, T. C. Ralph, and A. I. Lvovsky, Nat. Photonics **9**, 764 (2015).
[44] A. Dutt, K. Luke, S. Manipatruni, A. L. Gaeta, P. Nussenzveig, and M. Lipson, Phys. Rev. Applied **3**, 044005 (2015).
[45] Y. Zhao, Y. Okawachi, J. K. Jang, X. Ji, M. Lipson, and A. L. Gaeta, Phys. Rev. Lett. **124**, 193601 (2020).
[46] Y. Zhang, M. Menotti, K. Tan, V. D. Vaidya, D. H. Mahler, L. G. Helt, L. Zatti, M. Liscidini, B. Morrison, and Z. Vernon, Nat. Commun. **12**, 2233 (2021).
[47] V. D. Vaidya, B. Morrison, L. G. Helt, R. Shahrokhshahi, D. H. Mahler, M. J. Collins, K. Tan, J. Lavoie, A. Repingon, M. Menotti, N. Quesada, R. C. Pooser, A. E. Lita, T. Gerrits, S. W. Nam, and Z. Vernon, Sci. Adv. **6**, eaba9186 (2020).
[48] F. Lenzini, J. Janousek, O. Thearle, M. Villa, B. Haylock, S. Kasture, L. Cui, H.-P. Phan, D. V. Dao, H. Yonezawa, P. K. Lam, E. H. Huntington, and M. Lobino, Sci. Adv. **4**, eaat9331 (2018).
[49] T. Kashiwazaki, N. Takanashi, T. Yamashima, T. Kazama, K. Enbutsu, R. Kasahara, T. Umeki, and A. Furusawa, APL Photonics **5**, 036104 (2020).